J Mater Sci (2008) 43:551–556
DOI 10.1007/s10853-007-1714-7

5TH BRAZILIAN MRS MEETING

Lanthanum-based perovskites obtained by the polymeric precursor method

Danniely S. Melo · Érika P. Marinho · Luiz E. B. Soledade · Dulce Maria A. Melo · Severino Jackson G. Lima · Elson Longo · Iêda Maria Garcia Santos · Antonio G. Souza

Received: 22 December 2006 / Accepted: 21 March 2007 / Published online: 28 June 2007

Abstract Cobalt oxides, specially the ones with perovskite structure, are of a high technological interest, due to their interesting optical, electrical and magnetic properties. $La_{1-x}Ca_xCoO_3$ powder samples were synthesized by the polymeric precursor method, with x varying from 0 to 0.4. The powder precursors were characterized by TG/DTA, XRD and IR. The TG curves showed several thermal decomposition steps; the first one is ascribed to the loss of water and the remaining steps are related to the combustion of the organic matter. The XRD patterns indicated only the presence of the perovskite phase. Moreover, the structure changes from rhombohedral to cubic, as calcium is added to the perovskite and the calcination temperature increases.

D. S. Melo (✉) · É. P. Marinho · L. E. B. Soledade · I. M. G. Santos · A. G. Souza
Laboratório de Combustíveis e Materiais, Departamento de Química, Universidade Federal da Paraíba, Joao Pessoa, PB, Brazil
e-mail: dannielym@yahoo.com.br

D. M. A. Melo
Departamento de Química, Universidade Federal do Rio Grande do Norte, Campus I, Natal, RN, Brazil

S. J. G. Lima
Laboratório de Solidificação Rápida, Departamento de Tecnologia Mecânica, Universidade Federal da Paraíba, Joao Pessoa, PB, Brazil

E. Longo
CMDMC, Instituto de Química, UNESP-Araraquara, Araraquara, SP, Brazil

Introduction

The interest in studying ceramic oxides with perovskite structure has been motivated by their interesting optical, electric and magnetic properties [1]. These materials can be applied as gas sensors, thermal electric batteries, chemical sensors, fuel cells and also as catalysts in the reactions of CO oxidation, CO and NO_x decomposition and the combustion of methane and propane [2–4]. The properties of these oxides strongly depend on the synthesis method [4].

The ideal perovskite structure presents the ABO_3 stoichiometry, with a cubic close-packing. In the perovskites, the larger and more ionic A cation is coordinated by 12 oxygen ions, whereas the smaller and more covalent B cation is coordinated by 6, displaying an octahedral geometry [5, 6]. However, this structure is frequently distorted, leading to tetragonal, orthorhombic and rhombohedral structures [1].

The interest in the $LaCoO_3$ perovskite is due to the high electronic and ionic conductivity, when divalent cations substitutes for La [7]. Much attention has been paid to lanthanum perovskites ($LaMO_3$, in which M=Co or Mn), due to their high catalytic activity and thermal stability in the hydrocarbon oxidation reactions. These perovskites even achieve activities as high as the ones from noble metal catalysts. The Ca substitution for La, in the 12-fold oxygen-coordinated A sites, does not alter the fundamental perovskite structure [1]. Such substitution leads to oxygen vacancies and/or stabilizes the uncommon 3^+ valence of the cation occupying the B octahedral sites [8, 9], enhancing the system catalytic properties.

In the present work, $LaCoO_3$:Ca perovskites were synthesized by the polymeric precursor method. This method consists in the formation of a chelate of the cations with an α-hydroxycarboxylic acid, more often citric acid [10].

Later, a polyhydroxy alcohol, generally ethylene glycol, is added. Upon heating, the polyesterification reaction takes place. A primary heating in an oxydizing atmosphere at about 250–300 °C produces the so-called powder precursor. The heat treatment of the powder precursor at an adequate temperature yields a ceramic powder, with a higher quality than the powders synthesized by solid state reaction [11]. At the relatively low temperature used in such method, other synthesis methods produce low crystallinity powders, displaying secondary phases [12]. The polymeric precursor method presents also other advantages such as good homogeneity, good stoichiometric control and good control of the particle morphology [11, 13, 14].

Experimental

$La_{1-x}Ca_xCoO_3$ powder samples were synthesized by the polymeric precursor method, with $x = 0$, 0.2 and 0.4. In the synthesis, the following reagents, with purities ranging from 98 to 99.9%, were used: citric acid (Cargill), lanthanum nitrate (Sigma), calcium nitrate (Vetec), cobalt nitrate (Vetec) and ethylene glycol (Vetec). The synthesis procedure is described in Fig. 1, in which a 3:1 citric acid to metal molar ratio was employed. A mass proportion of 60% citric acid to 40% ethylene glycol was used.

The TG and DTA analyses of the powder precursors were performed in a SDT 2960 TA Instruments analyzer, with a heating rate of 10 °C min^{-1} up to 900 °C, in a synthetic air atmosphere, using alumina crucibles.

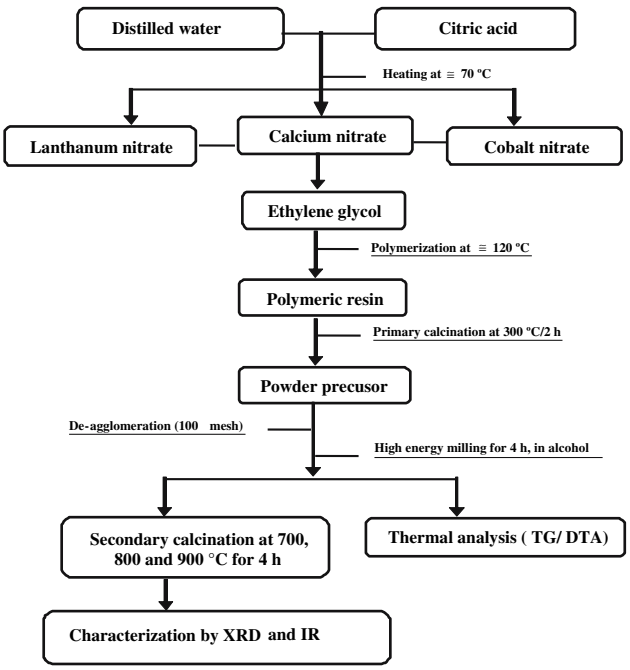

Fig. 1 Flowchart for the synthesis of the $La_{1-x}Ca_xCoO_3$ samples, using the polymeric precursor method

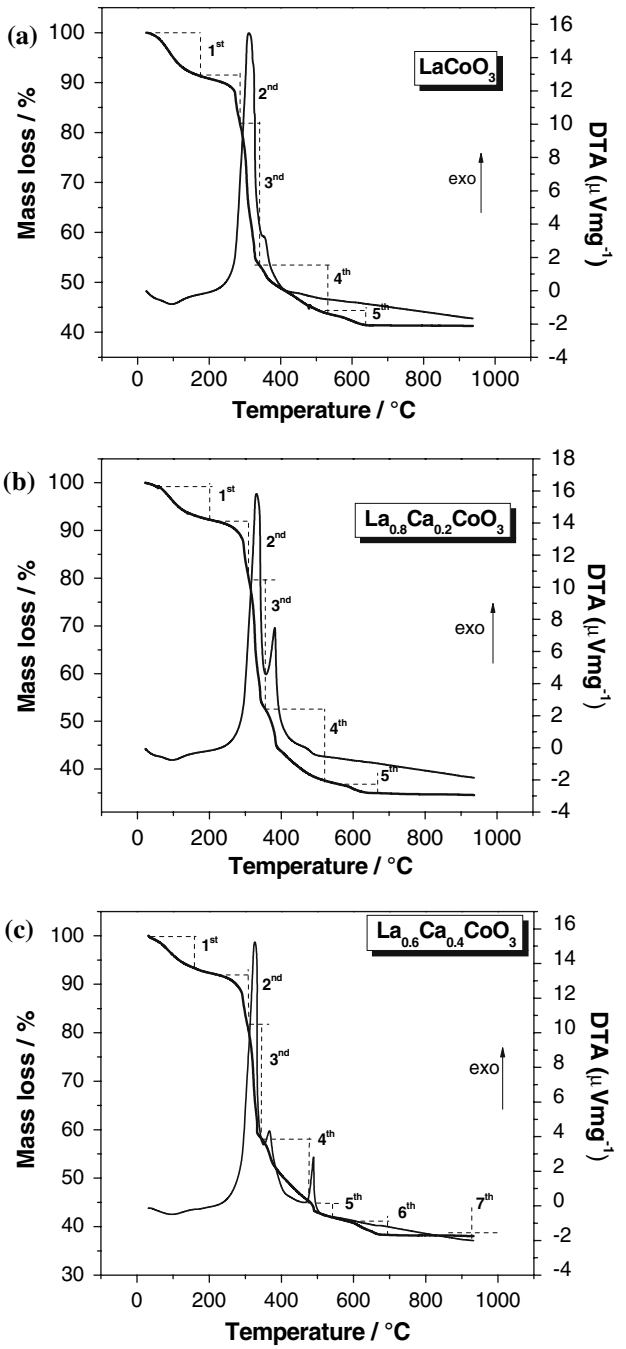

Fig. 2 TG and DTA curves of the $La_{1-x}Ca_xCoO_3$ powder precursors. (**a**) $LaCoO_3$, (**b**) $La_{0.8}Ca_{0.2}CoO_3$ and (**c**) $La_{0.6}Ca_{0.4}CoO_3$

The $La_{1-x}Ca_xCoO_3$ samples were characterized by X-ray diffraction in a D-5000 Siemens diffractometer, with a step size of 0.03° and step time of 1 s, using the CuK_α radiation (λ= 1.54060 Å) and 2θ values ranging from 20 to 80°.

The FTIR spectra were obtained in the range from 2,000 to 400 cm^{-1}. The samples were previously pressed in KBr and analyzed in a MB 102 Bomem spectrophotometer.

Results and discussion

The TG and DTA curves of the $La_{1-x}Ca_xCoO_3$ precursors are presented in Fig. 2a–c, and the thermoanalytical results are summarized in Table 1. In most samples, the thermal decomposition occurs in five steps. In all samples, the first step takes place below 200 °C and presents a small mass loss, ascribed to the loss of water and some adsorbed gases. Generally, the other steps are associated to the combustion of the organic matter.

The TG curve related to the $La_{0.6}Ca_{0.4}CoO_3$ sample presents a sixth thermal decomposition step, which is related to the presence of carbonates. At about 800 °C, a small mass loss is observed, probably related to the carbonate decomposition [12].

All the DTA curves display a main exothermic peak, in the region from 300 to 340 °C, ascribed to the combustion of the organic matter, associated to the polymeric precursor method. For the Ca-free sample, a small shoulder is noticed at 352 °C, probably related to the residual carbon [12]. A similar behavior was observed for the samples with the Ca substitution for La, but in this case well defined peaks are noticed: one peak at 382 °C for $La_{0.8}Ca_{0.2}CoO_3$ and two peaks at 367 and 489 °C for $La_{0.6}Ca_{0.4}CoO_3$. This second peak is assigned to the decomposition of refractory organic material.

The XRD patterns are presented in Fig. 3. The majority of the XRD patterns only indicated the presence of the perovskite phase, with cubic or rhombohedral structure, according to JCPDS files 01-075-0279 and 01-084-0848, respectively. The exception was the $La_{0.6}Ca_{0.4}CoO_3$ sample, heat treated at 700 °C, which also presented peaks assigned to calcite. At higher temperatures, the calcite

Table 1 Temperature and mass losses determined by TG

	Step	T_i (°C)	T_p (°C)	T_f (°C)	Mass loss (%)
$LaCoO_3$	1st	28	88	175	8.6
	2nd	175	277	286	9.4
	3rd	286	305	340	28.4
	4th	340	357	530	9.7
	5th	530	584	656	2.4
$La_{0.8}Ca_{0.2}CoO_3$	1st	57	90	198	6.7
	2nd	217	298	308	11.3
	3rd	308	326	353	27.8
	4th	353	382	517	15.2
	5th	566	595	652	1.7
$La_{0.6}Ca_{0.4}CoO_3$	1st	44	87	155	5.9
	2nd	223	296	305	10.1
	3rd	305	322	342	23.5
	4th	342	368	472	12.9
	5th	472	488	538	3.5
	6th	584	615	689	2.8
	7th	877	–	933	0.2

T_i = initial temperature, T_p = peak temperature, T_f = final temperature

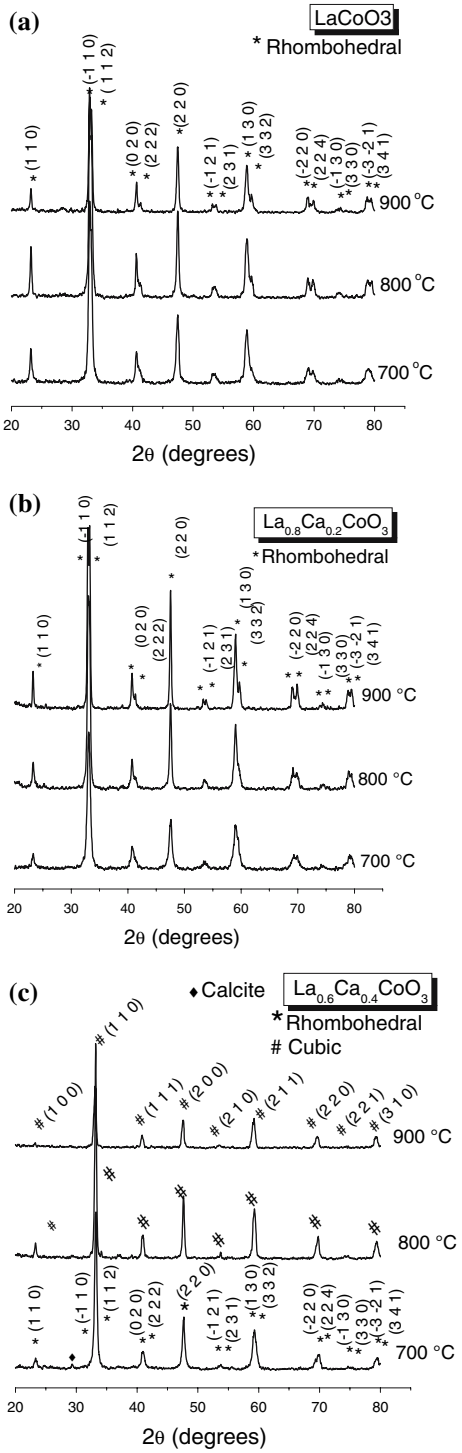

Fig. 3 XRD patterns of the $La_{1-x}Ca_xCoO_3$ samples, heat treated at 700, 800 and 900 °C, (**a**) $LaCoO_3$, (**b**) $La_{0.8}Ca_{0.2}CoO_3$ and (**c**) $La_{0.6}Ca_{0.4}CoO_3$

peaks disappear, due to the carbonate decomposition, as pointed out by the thermogravimetric data.

Thus, the use of the polymeric precursor method was successful in the synthesis of single phase $La_{1-x}Ca_xCoO_3$ samples. According to Orlovskaya et al. this is a difficult synthesis, and the presence of secondary phases is usual, altering the material properties [7].

The $LaCoO_3$ powder samples presented rhombohedral structures at all heat treatment temperatures. Higher heat treatment temperatures and associated to higher calcium additions led to the stabilization of the cubic structure, as shown in the XRD patterns, in agreement with Orlovskaya et al. [15]. This result is confirmed by the deconvolution curves of the XRD patterns, after calcination at 700 °C (Fig. 4). The bifurcation of the peak placed at around 70° is characteristic of the rhombohedral phase—this behavior is observed in all samples with rhombohedral structure. On the other hand, this bifurcation was not observed in the sample $La_{0.6}Ca_{0.4}CoO_3$ calcined at 900 °C, indicating that a cubic phase is present.

The lattice parameters of the perovskites were calculated from the X-ray diffraction patterns using the Rede 93 program, developed by Paiva Santos et al. [16]. Based on XRD patterns, the values of full width at half maximum (FWHM) and lattice parameters were calculated, and are depicted in Table 2. Most of the results of the present work agree with the data of the JCPDS file, which are: $a = b = c = 5.37780$ Å and $\alpha = \beta = \gamma = 60.80°$, for the rhombohedral structure and $a = b = c = 3.82000$ Å and $\alpha = \beta = \gamma = 90°$, for the cubic structure. It may be observed that, in the present work, the rhombohedral samples present angles close to 90°, tending to the cubic structure, thus indicating that a higher long range order occurs, with a more symmetric structure.

The $LaCoO_3$ sample presented the highest FWHM value, indicating the lowest long range order. Upon the calcium addition, a higher short range disorder occurs, as two different cations occupy the same 12-fold oxygen-coordinated sites. The defects formed are presented in Eq. 1. It may be observed that 11-fold oxygen-coordinated Ca^{2+} polyhedra are formed, besides the usual 12-fold oxygen-coordinated Ca^{2+} polyhedra. As a consequence, ordered–disordered phases are formed, with two types of coordination for the calcium ions, with the formation of clusters. Moreover, oxygen vacancies can occur in three different charge states: the $\left\lfloor CaO_{11} \cdot V_O^x \right\rfloor_{complex}$ state, which has captured electrons and is neutral relative to the lattice (donor state), the $\left\lfloor CaO_{11} \cdot V_O^{\circ\circ} \right\rfloor_{complex}$ state, which did not trap any electron and is doubly positively charged with respect to the lattice (acceptor state) and the singly ionized $\left\lfloor CaO_{11} \cdot V_O^{\circ} \right\rfloor_{complex}$ state (donor or acceptor state). Therefore, most of the oxygen vacancies are vacancy complexes in ordered–disordered structure. As a consequence of this ordered–disordered structure, the system tends to a higher

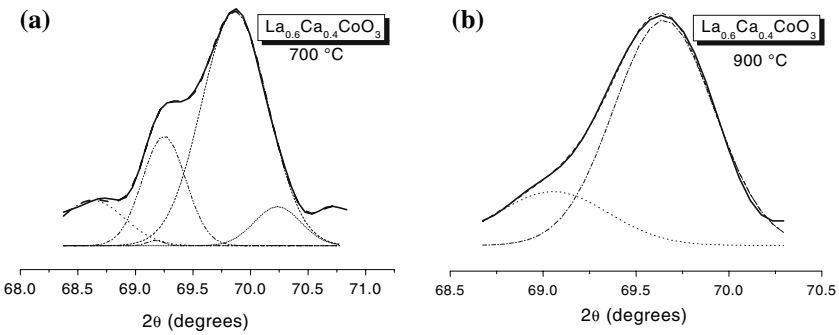

Fig. 4 Examples of deconvolution of the XRD patterns of the sample $La_{0.6}Ca_{0.4}CoO_3$ heat treated at: (**a**) 700 °C and (**b**) 900 °C

Table 2 Lattice parameters and FWHM values of the system $La_{1-x}Ca_xCoO_3$

		$a = b = c$ (Å)	$\alpha = \beta = \gamma$ (°)	FWHM (°)	Diffraction plane for the calculation of the FWHM values
$LaCoO_3$	700 °C	5.381	89.511	0.69	(–1 10) and (1 1 2)
	800 °C	5.383	89.512	0.62	(–1 10) and (1 1 2)
	900 °C	5.383	89.512	0.66	(–1 10) and (1 1 2)
$La_{0.8}Ca_{0.2}CoO_3$	700 °C	5.352	89.498	0.65	(–1 10) and (1 1 2)
	800 °C	5.355	89.499	0.57	(–1 10) and (1 1 2)
	900 °C	5.376	89.511	0.61	(–1 10) and (1 1 2)
$La_{0.6}Ca_{0.4}CoO_3$	700 °C	5.357	89.499	0.48	(–1 10) and (1 1 2)
	800 °C	3.815	90	0.41	(1 10)
	900 °C	3.819	90	0.40	(1 10)

long range order (lower FWHM values), and the phase transition from rhombohedral to cubic occurs.

$$
\begin{aligned}
&2CaO \overset{LaCoO_3}{\longrightarrow} 2Ca'_{La} + V_O^{\circ\circ} + 2O_O^x \\
&\left[CaO_{11}\cdot V_O^x\right]_c + \left[CaO_{12}\right]_c^x \rightarrow \left[CaO_{11}\cdot V_O^\circ\right]_c + \left[CaO_{12}\right]_c' \\
&\left[CaO_{11}\cdot V_O^x\right]_c + \left[LaO_{12}\right]_c^x \rightarrow \left[CaO_{11}\cdot V_O^\circ\right]_c + \left[LaO_{12}\right]_c' \\
&\left[CaO_{11}\cdot V_O^\circ\right]_c + \left[CaO_{12}\right]_c^x \rightarrow \left[CaO_{11}\cdot V_O^{\circ\circ}\right]_c + \left[CaO_{12}\right]_c' \\
&\left[CaO_{11}\cdot V_O^\circ\right]_c + \left[LaO_{12}\right]_c^x \rightarrow \left[CaO_{11}\cdot V_O^{\circ\circ}\right]_c + \left[LaO_{12}\right]_c'
\end{aligned}
\tag{1}
$$

where c = complex.

In relation to temperature, the highest long range order was noticed for the heat treatment at 800 °C, decreasing for higher and lower temperatures. At 700 °C, the system is not fully organized and amorphous phase may still be present. At 800 °C, a high crystallinity is observed, with low amount of defects. At 900 °C, a reduction of Co^{3+} to Co^{2+} occurs, leading to the formation of defects, as presented in Eq. 2.

$$
\begin{aligned}
&2CoO \overset{LaCoO_3}{\longrightarrow} 2Co'_{Co} + V_O^{\circ\circ} + 2O_O^x \\
&\left[CoO_5\cdot V_O^x\right]_c + \left[CoO_6\right]_c^x \rightarrow \left[CoO_5\cdot V_O^\circ\right]_c + \left[CoO_6\right]_c' \\
&\left[CoO_5\cdot V_O^\circ\right]_c + \left[CoO_6\right]_c^x \rightarrow \left[CoO_5\cdot V_O^{\circ\circ}\right]_c + \left[CoO_6\right]_c'
\end{aligned}
\tag{2}
$$

where c = complex.

As in the previous case, two different Co polyhedra are observed, a 5-fold oxygen-coordinated and a 6-fold oxygen-coordinated polyhedra. As a consequence, most of the oxygen vacancies are vacancy complexes in ordered–disordered structure and three different charge states may be observed: $\left[CoO_5\cdot V_O^x\right]_{complex}$, $\left[CoO_5\cdot V_O^\circ\right]_{complex}$ and $\left[CoO_5\cdot V_O^{\circ\circ}\right]_{complex}$. In this case, the decrease in the symmetry is smaller than in calcium substitution, indicated the influence of this decrease in short range symmetry also influences the long range symmetry. Thus, for the sample $La_{0.6}Ca_{0.4}CoO_3$, a transition from rhombohedral to cubic is observed with the temperature increase—a rhombohedral structure was observed at 700 °C, whereas at 900 °C, the α values increase, approaching 90° and a cubic structure was noticed. It is no surprise that this sample displays the lowest FWHM values.

The sample $La_{0.8}Ca_{0.2}CoO_3$ displayed a FWHM which is not significantly different of the sample $LaCoO_3$. Thus for these samples, a small decrease in long range order occurs.

As a consequence of defect formation, $LaCoO_3$ and $La_{0.8}Ca_{0.2}CoO_3$ maintain the rhombohedral structure for the three calcination temperatures, whereas the sample $La_{0.6}Ca_{0.4}CoO_3$ is rhombohedral at 700 °C and cubic at higher temperatures.

The infrared spectra of the $La_{1-x}Ca_xCoO_3$ samples, heat treated at 700, 800 and 900 °C, are presented in Fig. 5. Bands related assigned to the metal-oxygen bond are observed at 600 and 480 cm^{-1} [17]. One band was observed at about 1,100 cm^{-1}, indicating the presence of hydroxo groups on the surface of the material. According to Nakamoto [18], the hydroxo group can be distinguished from the aquo group, since the former lacks the HOH bending mode near 1,600 cm^{-1}. Furthermore, the hydroxo complex exhibits the MOH bending mode below 1,200 cm^{-1}. Bands assigned to ester are also observed,

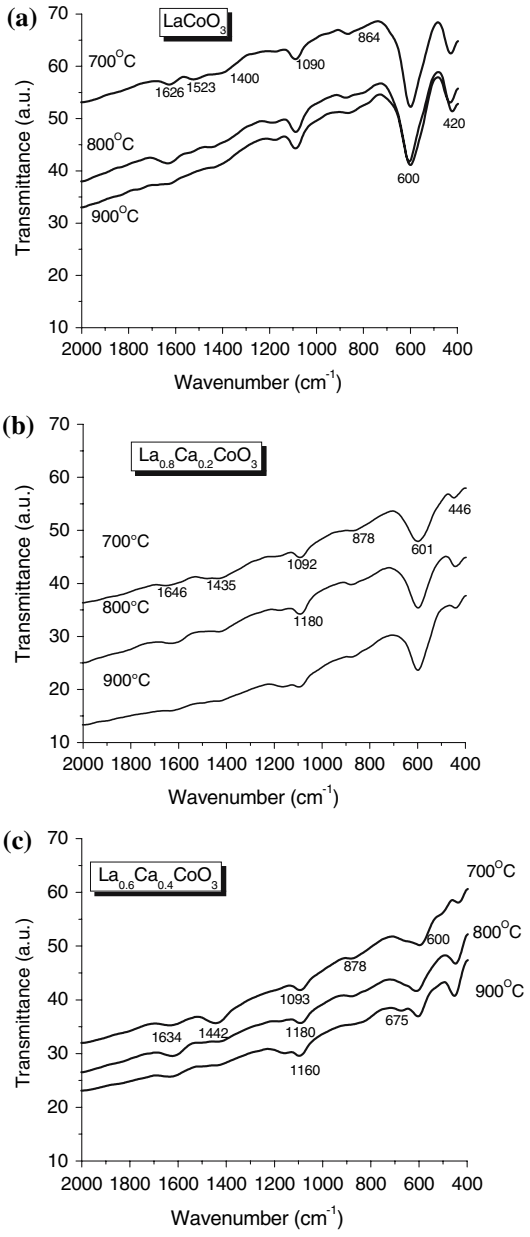

Fig. 5 Infrared spectra of the $La_{1-x}Ca_xCoO_3$ powder samples, heat treated at 700, 800 and 900 °C. (**a**) $LaCoO_3$, (**b**) $La_{0.8}Ca_{0.2}CoO_3$ and (**c**) $La_{0.6}Ca_{0.4}CoO_3$

being located at about 1,620 and 1,520 cm^{-1}, the first peak is assigned to ν(C=O), while the second is ascribed to ν(COO–). The intensity of the ester (COO–) bands decreases with the temperature increase. According to Nakayama et al. [17], carbonate bands are also observed, at 1,090 and 860 cm^{-1}, for samples calcined at 700 °C. The intensity of this band is higher for the system with 40% of calcium, which also presented carbonate peaks in XRD patterns. These carbonate bands also disappear with the temperature increase. These results are in agreement with the TG/DTG curves.

It should be observed that the bands related to metal-oxygen bonds broaden when calcium is added to the perovskite. This is related to the decrease in the short range order, as previously commented.

Conclusions

The polymeric precursor method was successfully used for the synthesis of single phase $La_{1-x}Ca_xCoO_3$ powders, at a relatively low temperature.

At 700 °C, carbonates were also observed, being decomposed at higher temperatures, leading to the presence of only the perovskite phase. Two different types of perovskite were obtained, rhombohedral and cubic, according the order–disorder structure formed in the material. Higher heat treatment temperatures and high calcium addition led to the stabilization of the cubic structure, due to the long range order–disorder structure. As a consequence, the samples $LaCoO_3$ and $La_{0.8}Ca_{0.2}CoO_3$ maintain the rhombohedral structure for the three calcination temperatures. Conversely, the sample $La_{0.6}Ca_{0.4}CoO_3$ changes from rhombohedral to cubic, with the increase of temperature from 800 to 900 °C.

Acknowledgements The authors acknowledge the Brazilian research funding agencies CNPq and CAPES for the financial support to this work.

References

1. Silva PRN (2004) Quim Nova 27:35
2. Haas O, Struis RPWJ, Mcbreen JM (2004) J Solid State Chem 177:1000
3. Spinicci R, Delmastro A, Ronchetti S, Tofanari A (2002) Mater Chem Phys 78:393
4. Popa M, Frantti J, Kakihana M (2002) Solid State Ionics 154:135
5. De Florio DZ, Fonseca FC, Muccillo ENS, Muchillo R (2004) Cerâmica 275:50
6. Spinicci R, Tofanari A, Faticanti M, Pettiti I, Porta P (2001) J Mol Catal A-Chem 176:247
7. Orlovskaya N, Kleveland K, Grande T, Einarsrud M (2000) J Eur Ceram Soc 20:51
8. Martinez-Ortega F, Batiot-Dupeyrat C, Valderrama G, Tatibouët JM (2001) C R Acad Sci Paris, Serie IIc, Chimie: Chemistry 4:49
9. Stojanovic M, Haverkamp RG, Mims CA, Moudallal H, Jacobson AJ (1997) J Catal 165:315
10. Candeia RA, Bernardi MIB, Longo E, Santos IMG, Souza AG (2004) Mater Lett 58:569
11. Gouveia DS, Souza AG, De Maurera MAMA, Da Costa CEF, Santos IMG, Prasad S, De Lima JB, Paskocimas CA, Longo E (2002) J Therm Anal Cal 67:459
12. Popa M, Kakihana M (2002) Solid State Ionics 151:251
13. Gouveia DS, Rosenhaim R, De Maurera MAMA, Lima SJG, Paskocimas CA, Longo E, Souza AG, Santos IMG (2004) J Therm Anal Cal 75:453
14. Souza SC, Souza MAF, Lima SJG, Santos MRC, Fernandes Jr. VJ, Soledade LEB, Longo E, Souza AG, Santos IMG (2005) J Therm Anal Cal 79:455
15. Orlovskaya N, Gogotsi Y, Reeco M, Cheng B, Gibson I (2002) Acta Mater 50:715
16. Paiva-Santos CO, Garcia D, Mascarenhan YP, Eiras JA (1989) Assoc Bras Ceram 35:153
17. Nakayama S, Okazaki M, Aung YL, Sakamoto M (2003) Solid State Ionics 158:133
18. Nakamoto K (1980) Infrared and Raman spectra of inorganic and coordination compounds. John Wiley and Sons, New York